Journal of Imaging Science and Technology® 54(3): 030504–030504-6, 2010.

Sheet Transport Simulation for Electrostatic Transfer Process in Electrophotography[1]

T. Sasaki, K. Yamamoto, T. Onishi and A. Sugiyama
Analysis Technology Center, Canon Inc., Tokyo, Japan
E-mail: sasaki.toyoshige@canon.co.jp

T. Tomizawa
Office Imaging Products Device Development Center, Canon Inc., Ibaraki, Japan

Y. Yoda
Peripherals Development Center, Canon Inc., Shizuoka, Japan

Abstract. *In the transfer process of electrophotography, electrostatic forces caused by the transfer electric field act on a sheet in the nip region. As a result, the sheet sticks to the photoconductor drum and sheet transport fails. The authors have developed a numerical simulation method of sheet transport in the transfer process. The method calculates sheet transport by means of weak coupling between electric field and structural analyses and considers electrostatic forces acting on the sheet and displacement of components relative to each other. The authors used the method to calculate sheet transport in a system that consists of two rollers and the sheet between them. In this system, the sheet passes between two rollers which contact each other and to which a voltage is applied. The calculated charge density, discharges, and sheet displacement showed good agreement with experiments. Another analysis clarified the relationship between electric discharges in the nip region and the sheet sticking to the roller. © 2010 Society for Imaging Science and Technology.*
[DOI: 10.2352/J.ImagingSci.Technol.2010.54.3.030504]

INTRODUCTION

In electrophotographic systems such as printers or copiers, the roller transfer system is commonly used for ecological reasons. Figure 1 shows the principle of the roller transfer system applied to monochrome electrophotography. The transfer roller is kept pressed against the photoconductor drum, and a paper sheet is inserted between the roller and the drum. The photoconductor drum is kept grounded, and a positive voltage is impressed on the transfer roller. The negatively charged toners on the photoconductor drum are transferred onto the sheet by transfer electric field at the nip region and maintained stably on the sheet by the positive charges in the sheet which are supplied by the electric conduction and the discharges from the transfer roller.

One of the problems that may occur in the transfer process is defective transport of the sheet. In Fig. 1, the positive charge supplied from the transfer roller to the sheet may not be equivalent to the negative charge of the toner. Meanwhile the sheet may be supplied with negative charge from the photoconductor drum by discharges. As a result, the sheet becomes charged due to the unbalance of positive and negative charge. Electrostatic forces caused by the electric field in the transfer area act on the charged sheet as it passes through the nip region. These forces may cause the sheet to wind around the photoconductor drum or the transfer roller and result in defective transport of the sheet.

One study has investigated the electrostatic forces operating on the sheet by electric field analysis. In this way it developed a structural analysis and calculated sheet deformation.[1,2] However, the sheet deformation depends on the electric charges on the sheet influenced by the deformation of the sheet. Therefore, we must consider both the electric charges and the deformation of the sheet in order to calculate sheet transport precisely.

In this article, we developed a numerical simulation method, assessed its reliability, and clarified the mechanism by which a sheet sticks to a roller.

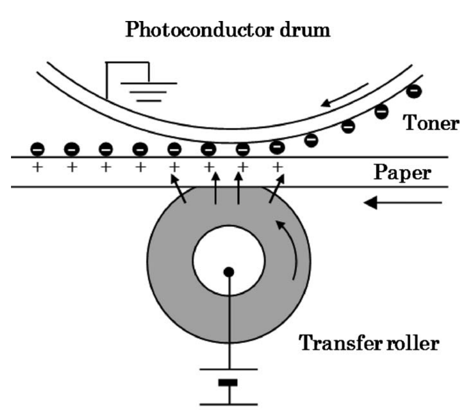

Figure 1. Principle of roller transfer system.

[1]Presented in part at IS&T's NIP24, Pittsburgh, PA, September 2008.

Received Mar. 25, 2009; accepted for publication Feb. 2, 2010; published online Apr. 15, 2010.
1062-3701/2010/54(3)/030504/6/$20.00.

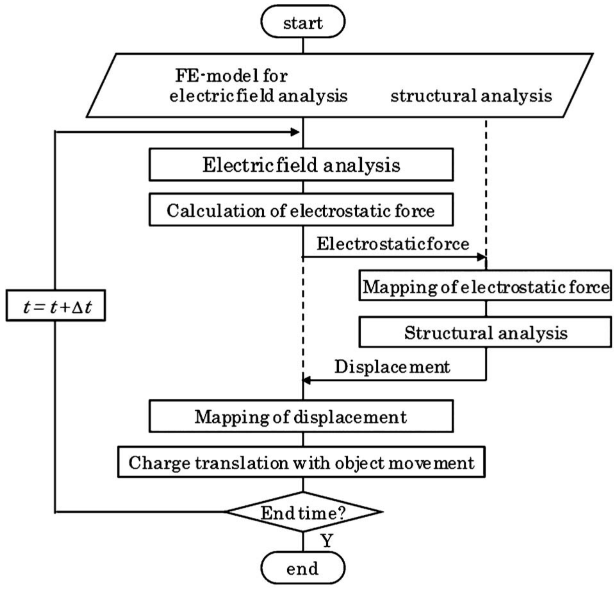

Figure 2. Simulation flowchart.

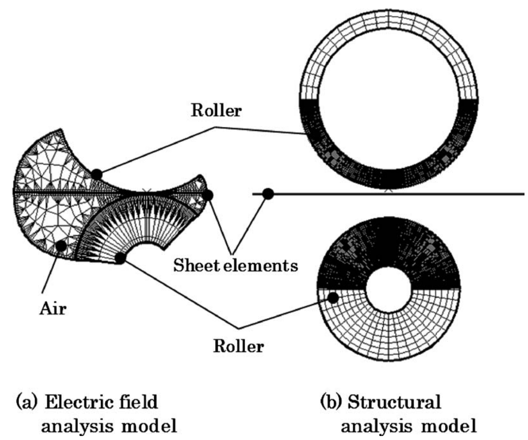

Figure 3. The simulation FE models.

SIMULATION METHOD

Calculation Flow

We developed a program to calculate sheet transport, and Figure 2 illustrates a flowchart of the program. This program weak-couples the electric field analysis and the structural analysis based on the finite element method. The boundary element method may be useful for electric field calculation; however, in this experiment, we need to obtain the discharge current and also consider the electric field nonlinearity of the conductivity (although this report shows only linearity). Of all factors considered, the finite element method works the best in this experiment.

This simulation is done on a two-dimensional cross section as shown in Fig. 1. The lengths of the photoconductor drum and transfer roller in the axis direction are much longer than their diameters, and the width of the paper is much longer than its thickness. Therefore, the two-dimensional approximation of the transfer system should be valid.

1. The program embodies two finite element models (FE models): one for the electric field analysis and the other for the structural analysis. Each FE model is shown in Figure 3. In the electric field analysis, the air also needs to be divided into finite elements. Furthermore, the elements near the nip region need to be divided more finely in order to consider the electric discharges in the microgap. The mesh is as fine as 5 μm around the gap by the nip region in this model, in consideration of the minimum discharge gap. This mesh influences the amount of discharge that both the obverse and reverse sides of the sheet receive. For that reason, two different FE models are used in the electric field and structural analyses.
2. The electric field analysis is performed taking into consideration electric conductivity and electric discharge. This makes it possible to calculate the distribution of the electric charge and the electric field.[3]
3. The program calculates the electrostatic force F acting on a sheet using Eq. (1):

$$F = (\sigma_A + \sigma_B)\frac{E_\alpha + E_\beta}{2}, \tag{1}$$

where σ_A, σ_B, E_α, and E_β are the surface charge densities on the obverse of the sheet, the reverse of the sheet, the electric field on the obverse of the sheet, and the electric field on the reverse of the sheet, respectively. This equation calculates the product of total sheet charges and the external electric field which is not caused by the sheet charges. This calculation is valid under the given condition where the boundary is at an infinite distance.

Equation (1) is applied to each node on the sheet surface in the FE model for the electric field analysis to calculate the distribution of electrostatic forces acting on the sheet.

4. The program maps the electrostatic forces. Electrostatic forces calculated for the nodes comprising the sheet in the FE model for electric field analysis using Eq. (1) are then transformed into those at the nodes composing the sheet in the FE model for the structural analysis.
5. The program performs the structural analysis in consideration of the electrostatic forces acting on the sheet in order to calculate the displacement of the nodes in individual components.
6. The program maps the displacement as follows. The displacement of nodes in the FE model for the structural analysis is transformed into that of nodes in the FE model for the electric field analysis. The nodes in the FE model for the electric field analysis move according to the displacement. In addition, the nodes in the air area also move according to the deformation of components as crushing elements do not form.

The program transfers charge on the surface of the object as the object advances. It then performs the electric field analysis using the FE model for electric field analysis after deformation and repeats the procedure described above.

Sheet Transport

As shown in Fig. 3, sheet elements must be prepared over the entire range of the analysis area in each FE model. In each calculation process, the following calculations are carried out according to the arrival position of the sheet at each time step.

In the electric field analysis, the surface node charges on the obverse and reverse of the sheet are transferred as the sheet advances, as mentioned above. With respect to the sheet elements in the FE model, the material properties of air or a roller are applied in an area which the sheet has not yet reached, whereas, in an area which the sheet has reached, the properties of the sheet itself are applied. The sheet transport is thus expressed by the transfer of node charge and the change in sheet element materials without changing FE mesh.

On the other hand, in the structural analysis, the sheet exists between two rollers that are separated. Then in each time step the analysis executes a static calculation of deformation where those two rollers sandwich the sheet. The rollers only sandwich the sheet and do not actually transfer it. Hence, an inertial force acting on the moving objective is not considered in this analysis. This simplified transfer process is based on our previous calculation that the shape of the medium is almost the same after either the medium is “transferred” by rollers or is “sandwiched” by rollers when the electric field is not considered. The implicit method is used in this calculation, and also the finite sliding contact method is utilized for objects in contact. This approach allows us to model sheet transport.

Simulation Program and Calculation Conditions

In this simulation program, the commercial code, ABAQUS, is applied for the part where it executes structural analysis, and for the rest, our original codes are applied. In a series of calculations that will be presented later in this article, the time step is set at 8 μs, which is sufficiently small compared to the time constant of the transfer roller. In this method, the sheet transfer distance measures 1.04 μm in each time step. The total step count is 40,000. After applying bias to the rollers and having the electric field in a stable state, we supply a sheet from the upstream nip region at 3 mm and transport it to the downstream nip region at 30 mm. The structural analysis is executed once in every 100 μm for which the sheet transports. This interval is selected on the basis of preliminary results which have shown that no matter how frequently structural analysis is executed, there is no difference for intervals below 100 μm. An Intel Xeon 3.8 MHz processor is used for the calculations, and it took around 8 h to finish each calculation. Note that no parallel processing is implemented in this calculation.

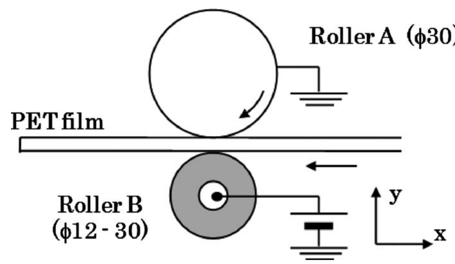

Figure 4. The test model.

Table I. Material properties.

	Roller A	Roller B	PET
Conductivity (S/m)	∞	3.0×10^{-7}	0
Relative permittivity		10	3
Young’s modulus (MPa)	5000	3	4000
Poisson’s ratio	0.35	0.49	0.3

RESULTS AND DISCUSSION

Experimental Model

Figure 4 shows the system for sheet transport. Roller B is kept pressed against roller A. A sheet is inserted between the two rollers and is transferred as roller A rotates. Roller A is made of metal, and its diameter is 30 mm. Roller B is made of rubber, and we use five kinds of rollers having different diameters. Both roller A and B are 8 cm long. The load applied to roller B is 1 kgf, and the voltage is applied to the shaft of roller B. A polyethylene terephthalate (PET) film is used as the sheet, and it moves at 130 mm/s. The material properties of each component are shown in Table I.

The PET film is charged only by electric discharges since PET is an insulator. The PET film accumulates negative charge by receiving electric discharges from roller A and accumulates positive charge by receiving electric discharges from roller B. The electric charges on the PET film are given by the sum of the charges on both sides of the film.

Charge on PET Film

We transferred a 100-μm-thick PET film while applying 3 kV to roller B, and measured the charge density on the PET film as follows. We set the PET film after transport on a grounded electrode, measured its surface potential, and converted it into charge density. The reason for using a 100-μm-thick PET film is to prevent the film from winding around the rollers. This strategy allows us to measure the surface potential easily. The experimental and calculation results are shown in Figure 5, revealing the relationship between the decrease in charge density and the increase in diameter of roller B.

Discharges

We compared the experiment and calculation on discharges under the conditions that the roller B diameter is 16 mm and applied voltage is 3 kV. Figures 6(a) and 6(b) show

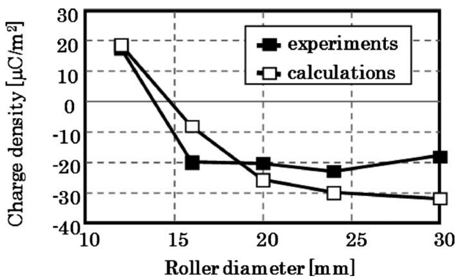

Figure 5. Relationship between the roller diameter and charge density on PET film.

results for 100-μm- and 50-μm-thick PET films being transferred, respectively. Black lines in the calculated result of the air gap represent discharges. The calculation agrees with the experiment in the following respects: when the PET film is 100 μm thick, discharges occur in the upper and lower nip region of rollers A and B, and the discharges in the upper nip region are stronger than in the lower nip region. When the PET film is 50 μm, the PET film winds around the roller A in both the experiment and calculation. This winding eliminates the air gap in the lower nip region. As a result, discharges take place between PET and roller B, which are weaker than the discharges in the upper nip region.

Sheet Deformation

We transferred a 50-μm-thick PET film while applying 2 kV to roller B and studied the deformation of the PET film. Figure 7 shows the condition of transport associated with the change in D, which is the sheet length from the center of the nip region to the tip of the sheet. Roller B diameter is 20 mm. Fig. 7(a) shows the experimental results, and Fig. 7(b) shows the calculation results, where contours and arrows are electric potential distribution and electrostatic forces acting on the sheet, respectively. Fig. 7(c), a close-up of the nip region from the calculation results, shows the condition of electric discharges. In Fig. 7(b), the PET film, after passing the nip region, winds around roller A. This result shows good agreement with the experiment in Fig. 7(a). The phenomenon is explained chronologically based on the calculation results. At $D=-2$ mm, the PETs tip is not reached the nip region. Thus, rollers A and B are electrically continuous with each other. At $D=1$ mm, the PETs tip slightly passes the nip region. In the upper nip region, the PET film re-

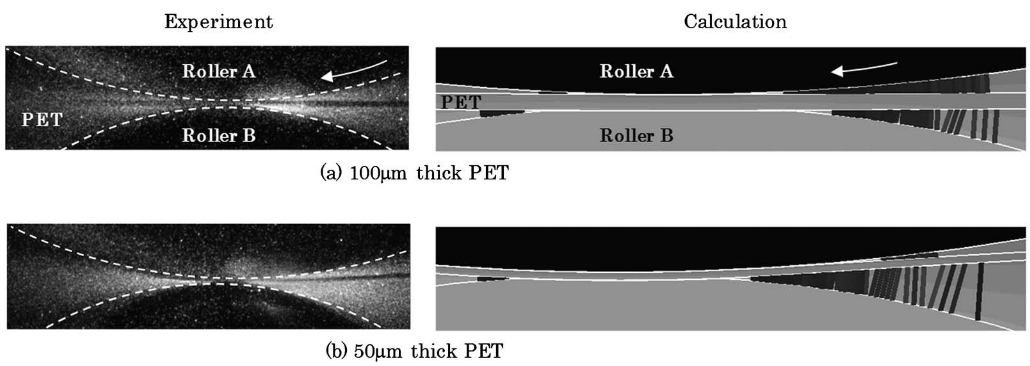

Figure 6. Comparison of discharges (roller $B=16$ mm, 3kV).

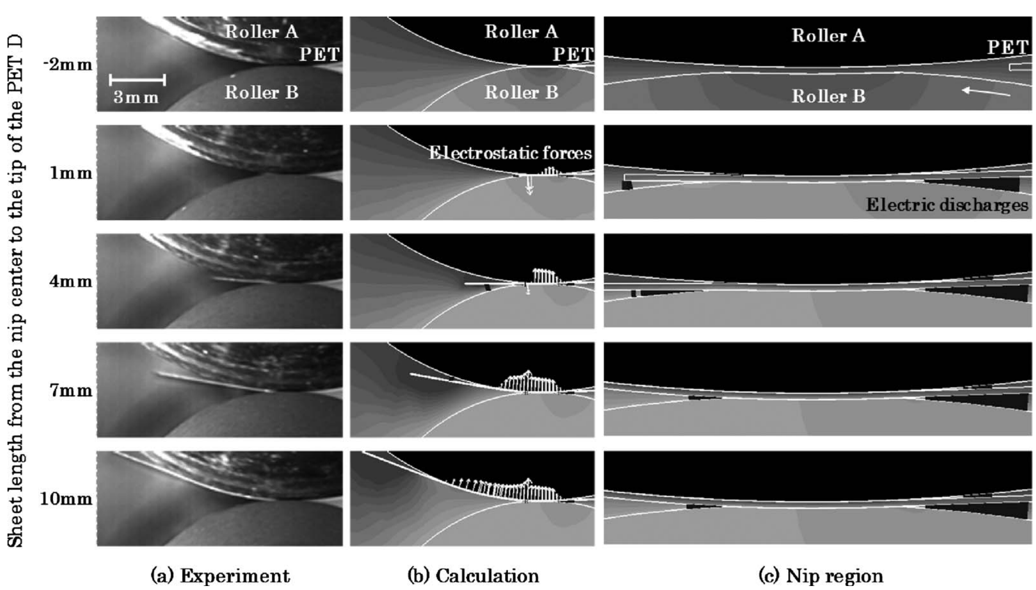

Figure 7. Comparison of PET transportation (roller $B=20$ mm, 2kV).

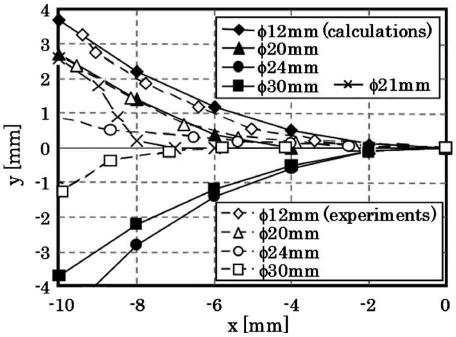

Figure 8. Trajectory of PETs tip.

ceives electric discharges on both surfaces. The direction of the electrostatic force acting on the PET film is toward roller A as the total electric charge is positive. On the contrary, in the lower nip region, the direction of the electrostatic force is acting toward roller B as the negative electric discharges are stronger when the PET film is receiving electric discharges on both surfaces. At $D=4$ mm, the part with positive charge in the upper nip region reaches the lower region. The PET film is still transported directly. At $D=7$ mm, the PET film begins to stick to roller A as the part with positive charge in the upper nip region passes through the lower region. Consequently, the air gap between roller A and the PET film disappears and electric discharges in the area vanish. This means that electric discharges in the lower nip region are only positive at this time. As a result, the sticking area extends rapidly until the sheet reaches $D=10$ mm.

Figure 8 compares the trajectories of the PET tip between experiment and calculation for various diameters of roller B. Coordinate axes are defined as shown in Fig. 4, and the origin exists at the center of the nip region. The calculated results and experimental results show the same tendency in the following respect. The sheet winds around roller A when the roller B diameter is 12 mm but tends to wind around roller B for larger diameters of roller B. This occurs because the negative discharges from roller A in both the upper and lower nip regions become more dominant with the larger roller diameter. The calculation results agree with the experimental ones for roller B at 12 or 20 mm but do not agree at 24 or 30 mm. This disagreement is probably caused by Young's modulus nonlinearity and the hysteresis of the roller B or the nonelectrostatic adhesion force between the roller and the sheet which this structural analysis to "sandwich" with rollers does not consider. It could also be that the assumption of Eq. (1), namely, that the boundary is at an infinite distance, is not valid. These factors perhaps contribute to the disagreement in this extremely delicate phenomenon where the sticking direction constantly changes.

Sheet Sticking

The experimental result for the 30 mm roller in Fig. 8 shows that the PET film winds around roller B rapidly after it is transferred nearly straight to the position $x=-8$ mm. This phenomenon often occurs in the development phase of the transfer process. Since it is very noticeable in the calculated result for the 21 mm roller also shown in Fig. 8, we came to the realization that we must analyze the cause and effect.

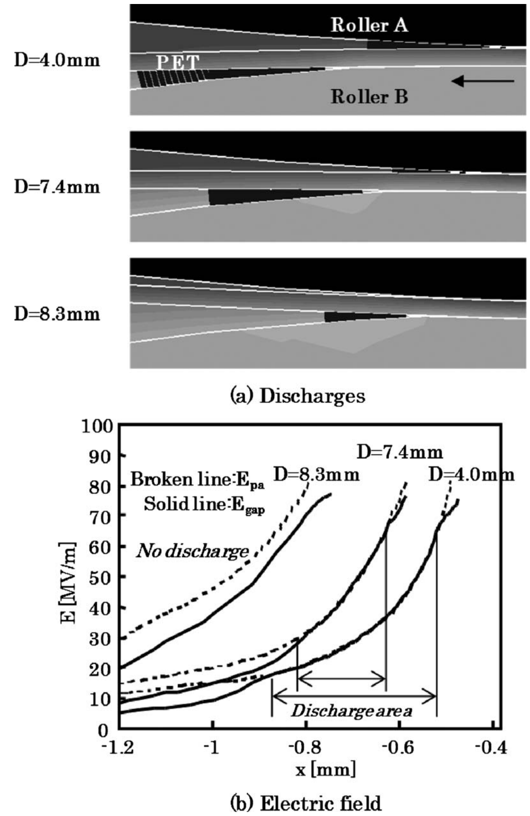

Figure 9. Electric discharges and electric field in the lower nipped region.

Figure 9 shows the transition in the lower nip region for the 21 mm roller: Fig. 9(a) shows the discharges and sheet deformation and Fig. 9(b) compares the change in the electric field between roller A and the PET film (E_{gap}) with the Paschen electric field ($E_{pa}=V_{pa}/\text{gap}$, where V_{pa} is Paschen's voltage). The condition of the PET film at each position is as follows. At $D=4$ mm, the area with positive charge in the upper nip region extends to the lower region. $D=7.4$ mm corresponds to the condition of the PET film right before beginning to wind rapidly. At $D=8.3$ mm, the PET film is winding. The electric field distribution in Fig. 9(a) shows that the gap between roller A and the PET film at $D=7.4$ mm is slightly shorter than that at $D=4$ mm. Although the electric discharges decrease, they still occur over a wide area. The electric field curve moves slightly toward the negative direction of the x axis because of the gap decrease as shown in Fig. 9(b). In addition, at $D=8.3$ mm, the curves of the electric field at the gap and the Paschen electric field separate from each other as shown in Fig. 9(b), and the electric discharges between roller A and the PET film disappear. Since the shape of the electric field curve is similar to that of the Paschen's curve, the electric discharges occurring in the lower nip region disappear rapidly. Therefore, the cause of the PET film winding rapidly is instantaneous disappearance of the negative electric discharges from roller A.

CONCLUSION

We developed a method of calculating sheet transport in the electrophotographic transfer process by means of weak coupling between electric field analysis and structural analysis by feeding back electrostatic forces and displacements between each of the analyses. We used this strategy to calculate the transport of a PET film, and the results qualitatively agreed with those of experiments. Further, we clarified the relationship between electric discharges in the nip region and sheet deformation.

REFERENCES

[1] T. Nagao, Z. Li, and N. Nakayama, "Analysis of paper deformation in electrophotography transfer process", *Proc. Japan Hardcopy 2003 Fall Meeting* (ISJ, Tokyo, 2003) pp. 53–56 (in Japanese).

[2] N. Nakayama and Y. Yimei, "Numerical study on sticking of paper in electrostatic transfer process for electrophotography", Int. J. Appl. Electromagn. Mech. **13**, 65–70 (2002).

[3] T. Sasaki, T. Onishi, A. Sugiyama, Y. Yoda, and T. Tomizawa, "Second transfer process simulation I", *Proc. IS&T's NIP24*, (IS&T, Springfield, VA, 2008) pp. 338–341.